Materials Research Express

PAPER • OPEN ACCESS

Effect of nano-Al_2O_3 addition on the microstructure and erosion wear of HVOF sprayed NiCrSiB coatings

To cite this article: Ayyappan Susila Praveen and Arun Arjunan 2020 *Mater. Res. Express* **7** 015006

Materials Research Express

PAPER

Effect of nano-Al_2O_3 addition on the microstructure and erosion wear of HVOF sprayed NiCrSiB coatings

Ayyappan Susila Praveen[1] **and Arun Arjunan**[2]

[1] Department of Mechanical Engineering, Vel Tech Rangarajan Dr Sagunthala R&D Institute of Science and Technology, Tamil Nadu, India

[2] School of Engineering, University of Wolverhampton, Telford Innovation Campus, TF2 9NT, United Kingdom

E-mail: a.arjunan@wlv.ac.uk

Keywords: nano-Al_2O_3, NiCrSiB coating, HVOF, coating

OPEN ACCESS

RECEIVED
27 October 2019

REVISED
24 November 2019

ACCEPTED FOR PUBLICATION
26 November 2019

PUBLISHED
9 December 2019

Abstract

Development of nanostructured high velocity oxy-fuel (HVOF) coatings with low porosity, high strength and increased wear resistance is still in its infancy. Combining nanoparticles with conventional microscale powders are increasingly being investigated to use with feedstock materials for thermal spray processes. Accordingly, this work investigates the addition of nano-Al_2O_3 particles on the microstructure and erosion wear of NiCrSiB HVOF coating in a stainless steel (AISI 304) substrate. Particle analysis of the NiCrSiB feedstock was conducted and the maximum allowable addition of Al_2O_3 nanoparticles have been identified using the 'mass mixture ratio' model considering both the particle size and density. Consequently, two cases are considered and their performance analysed: a maximum allowable case of 1.4 wt%, followed by a 0.17 wt% addition of nano-Al_2O_3 with NiCrSiB. Scanning Electron Microscope (SEM), Energy Dispersive Spectroscopy (EDS) and x-ray Diffraction (XRD) analysis were employed to inform the microstructure, material composition and phase spectrum of the resulting coatings. Subsequently, the nanostructured coating was exposed to both a pull-off adhesion strength test and hot air jet (450 °C) hard particle erosion to characterise its performance. It was found that the microhardness of the HVOF NiCrSiB coating improved from 576 $HV_{0.3}$ to 748 $HV_{0.3}$ with the addition of 1.4 wt% nano-Al_2O_3. Furthermore, the nanostructured coating also exhibited high erosion resistance at a 90° erodent impact angle. The increase in erosion wear resistance was due to the increase in the hardness as a result of the nano-Al_2O_3 addition.

1. Introduction

Solid particle erosion wear plays an important role in the material degradation process of engineering components [1–3], including turbines, thermal power plants, pipelines, hydropower machinery and combustion systems [4, 5]. According to Martinella [6], one of the major industries affected by solid particle erosion are coal based electric power plants. This is caused as a result of the fly ash interaction with the wall surfaces facilitated by the high-temperature flue gases. The prolonged effect of this causes the boiler components to fail and currently account for ~25% of the down time [7]. The subsequent cost effect of erosion wear damage in such cases is often as high as 54% of the overall maintenance cost [8, 9]. Consequently, coatings that can improve the surface resistance to solid particle erosion wear along with high-temperature oxidation protection systems are increasingly being sought.

Among the numerous solution available to prevent or control the fly ash erosion, surface coatings [10] are the most widely adopted technique [11–13]. When it comes to coating methodology, several techniques are available including vapour deposition [14], electrochemical, sol-gel [14] and thermal spraying [14]. Among these different coating techniques, thermal spray techniques [15, 16] have received increased attention largely due to their capacity to accommodate a range of coating powders and variety of substrate material [17, 18]. According to Ghadami *et al* [16], high velocity oxy-fuel (HVOF) is often favoured for high density coatings as

they feature a low flame temperature (<3000 K) at a high particle velocity (~500 m s^{-1}). Furthermore, HVOF also has high hardness, low degree of oxidation, and higher bond strength despite being comparatively cost effectiveness [19–21].

Over the years, a wide variety of coating materials have been successfully developed for use with thermal spraying technique. In that context, NiCrSiB coatings have gained popularity for wear and hot corrosion resistance, along with high-temperature oxidation. More importantly, the NiCrSiB coatings feature a low environmental impact [22–25] in comparison to other coatings of similar properties. The excellent properties to a large extend can be attributed to the formation of hard phases influenced by chromium (Cr), boron (B) and silicon (Si) which is then dispersed in the nickel (Ni) matrix. The self-fluxing properties of B and Si also lowers the melting temperature allowing for a lower energy usage [26, 27]. Despite the excllent wear and corrosion resistance of NiCrSiB coatings their lower hardness (in comparison to carbides and ceramics) makes them unsuitable for a range of industries. Consequently, the use of reinforcements are increasingly being sought to improve erosion-corrosion resistance of NiCrSiB coatings. In this regard, a range of micron-sized hard phases such as WC, CrC, TiC, SiC, Al_2O_3, Cr_3C_2, TiO_2, CeO_2 and ZrO_2 have been investigated to reinforce NiCrSiB [28–33].

Recently, the effect of nano-structuring on coatings have been investigated and significant improvement has been noticed in comparison to their micron-sized variants. Recently, Fernandes *et al* [34] combined nano-structured ZrO_2 to Ni-based alloy coating using atmospheric plasma spraying technique on a low carbon steel substrate. The subsequent sliding wear tests at room temperature showed that both the hardness and wear of coatings improved despite the decrease in friction coefficient. Addition of nano-Al_2O_3 particles to Ni-alloy coatings were carried out by Hou *et al* [35] using a plasma transferred arc overlay welding. It was found that a 0.8% (wt.) nanoscale Al_2O_3 raised the sliding wear resistance by 1.57 times. Addition of nano-Al_2O_3 to NiCrMoCu composite by Xu *et al* [36] through double glow plasma alloying on a stainless steel also showed excellent wear resistance. It was also reported that the wear weight loss of the composite alloying layer was 45% and 65% less than that of stainless steel and the NiCrMoCu respectively.

Wang *et al* [37] on the other hand studies a combination of Al_2O_3-SiC and nano-CeO_2 on the high temperature wear behaviour of Ni-alloy coatings produced by laser cladding. The results demonstrated the nano particles significantly increased the hardness of coatings (NiCoCrAlY: 350.5, NiCoCrAlY + Al_2O_3: 397.8, NiCoCrAlY + SiC: 484.9 and NiCoCrAlY + CeO_2: 385.7). A further comparative study using nano-CeO_2 and Sm_2O_3 to reinforce Ni through laser deposition was carried out by Zhang *et al* [38]; where an improvement in microhardness and wear-corrosion resistance was observed. Deposition of nano-Cr_2O_3 in combination with Ni-alloys on steel using duplex surface treatment was reported by Liu and Xu [39]. It was found that the Ni-Cr_2O_3 composite layer exhibited higher erosion-corrosion resistance. Furthermore, the slurry dynamic action was shown to not severely decrease the corrosion resistance and protective efficiency of the Ni-Cr_2O_3 layer.

Dispersion of a 1% mass-fraction nano-Al_2O_3 to create high-strength NiCoCrAlY superalloy coating by CO_2 laser was established by Wang *et al* [40]. This pioneering study aimed to quantify the 'nano-effect' of nanoscale Al_2O_3 particles; *i.e.* the nanos-size plays a substantial role in improving the microstructure of the coating itself. Other notable works include the use of activated-combustion high-velocity air-fuel (AC-HVAF) by Liu *et al* [41] to add nano-WC–12Co to WC–10Co–4Cr coatings. The subsequent slurry erosion test showed enhanced microhardness, wear and erosion resistance of the coated samples. The best performance was reported at a 15% addition of nano-WC–12Co to WC–10Co–4Cr.

While these studies validates the 'nano-effect' potential when it comes to developing high performance coatings, the influence of nonscale particle addition on the wear resistance of NiCrSiB coatings are yet to be established. Of particular interest, in this regard, is the effect of nano-Al_2O_3 addition on the microstructure, and erosion wear resistance of HVOF sprayed NiCrSiB coatings. The interest in adding nano-Al_2O_3 ceramic material is primarily due to its high level of hardness, wear and oxidation resistance. Accordingly, this study attempts to use nano-Al_2O_3 to reinforce Ni-based alloy coatings processed by HVOF thermal spraying technique. As opposed to plasma spraying, the HVOF technique is selected to demonstrate the suitability of the coating for high density applications. Accordingly, the nano-structured Al_2O_3-NiCrSiB coating will be deposited on an AISI304 stainless steel using HVOF spraying and the resulting performance in terms of microstructure, microhardness and erosion wear will be investigated.

2. Methodology

2.1. Substrate and coating feedstock

The deposition of coating feedstock was carried out on AISI304 stainless steel 25 × 25 × 6 mm substrate. The selection of AISI304 as the substrate of choice was due to its wide application in erosion-corrosion environment

Table 1. Chemical composition of AISI304 stainless steel.

Descriptions		Cr	Ni	Si	Mn	C	S	P	Fe
SS 304	Nominal	18–20	8–10.5	⩽1	⩽2	⩽0.08	⩽0.03	⩽0.045	Bal.
	Actual	18.736	8.288	0.366	1.440	0.023	0.006	0.029	Bal.

Table 2. Process parameters used for the HVOF thermal spray.

Parameters	Value
Oxygen gas flow rate	250 LPM
Oxygen gas pressure	8 kg cm^{-2}
LPG flow rate	60 LPM
LPG pressure	6 kg cm^{-2}
Air flow rate	650 LPM
Air pressure	5 kg cm^{-2}
Spray distance	250 mm
Powder feed rate	28 g min^{-1}

at high (>600 °C) service temperatures [8]. Particularly, the 304 variant is the most common boiler steel under both high temperature and oxidising environment [42, 43]. The coating surface of the substrate was manually grit blasted at 320–500 μm resulting in a surface roughness of approximately 9 $\pm$ 1 μm. According to Tillmann *et al* a surface roughness (~9 μm) can improve coating adhesions by promoting material interlocking between the feedstock and the substrate material. A case also validated by Sen *et al* [44] and Wang *et al* [45] while preparing their respective samples for nano-particle reinforced coating. In order to remove any contaminants that may have been introduced during the grit blasting process, the substrate was subsequently cleaned in acetone following an ultrasonic bath. Optical emission spectroscopy (ASTME 1086-08) was employed to evaluate the chemical composition of the substrate material; the results of which are presented in table 1.

Regarding the coating feedstock, micron sized NiCrSiB along with nano sized Al_2O_3 (hereafter referred to as nano-Al_2O_3) powders were the choice of materials. Particle size characterization of the feedstock was carried out and found that the NiCrSiB and nano-Al_2O_3 powder feature an average size D50 of 20 μm (micrometre) and 45 nm (nanometre) respectively. The nominal particle size distribution of the feedstock was characterised using the well-established laser diffraction technique using a Malvern Mastersizer 2000 (UK) following ASTM C1070 [46].

2.2. Coating procedure

HVOF has been regarded as one of the most efficient techniques for depositing high-performance coatings at moderate cost [47]. The procedure starts with the use of a carrier gas to transfer the feedstock powders into a combustion chamber. The feedstock is then heated to a high temperature as a result of the combustion of mixture gas. The molten and semi-molted particles are then accelerated by the combustible gases at supersonic velocity through a nozzle, subsequently being deposited on the substrate material resulting in a coating [48].

The general consensus is that HVOF is the most suitable methedology for NiCr [49–51] or WC-Co-based [52, 53] coatings, to improve both wear and oxidation resistance at an industrial scale. The HVOF system adopted in this study heats the feedstock using a mixtures of oxygen and liquified petroleum gas (LPG). Although multitude of fuels such as hydrogen, methane, propane, propylene, acetylene, natural gas and kerosene maybe used in compatible systems. The use of hydrogen is known to result in enhanced coating quality. However, this comes at a higher price; consequently the use of hydrogen is hard to justify when the particular coating application is not targeted at demonstrating the highest quality. The scope of this research is limited to studying the influence of nano-Al_2O_3 addition on the coating quality. Consequently, since all the coating cases being compared are conducted under consistent process parameters, the use of LPG is adequate. Table 2 summarises the HVOF process parameters used to generate the NiCrSiB + 1.4 wt% nano-Al_2O_3 coating at a constant thickness of 250 $\pm$ 30 μm.

2.3. Coating characterisation

The key properties relating to the mechanical performance of the coated surface are the microhardness and the adhesion strength. Consequently, both microhardness and adhesion strength measurements were carried out for all the coated samples. The microhardness (HV) tests were carried out using a Wilson-402MVD (Buehler) at 300-g load (15 s.). The stud pull adhesion tests were performed using a 14.2 mm (dia.) aluminium stud glued to

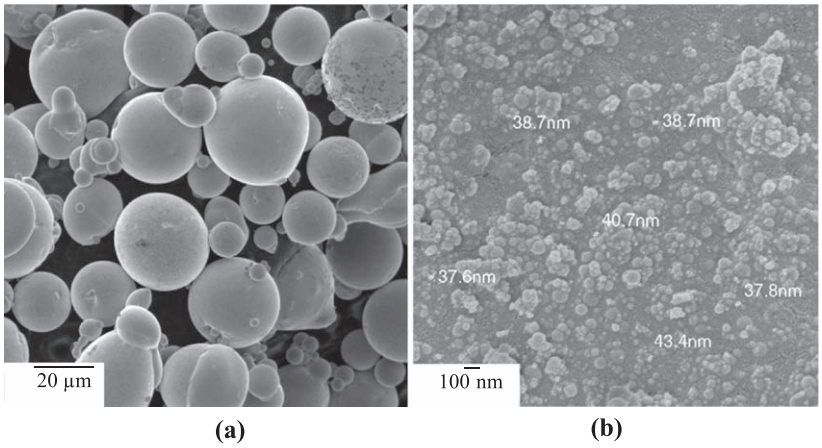

Figure 1. Scanning electron microscopy of particle size distribution for (a) NiCrSiB and (b) nano-Al_2O_3.

the coating using an epoxy paste; the assembly was oven cured at 150 °C (3 h.) following best practice reported by Elmoursi and Patel [54]. In order to ensure consistency, three samples were prepared and tested under identical conditions using an Elcometer-506 pull-off adhesion strength tester.

Quantification of the coating porosity was carried out through optical microscopy investigation of the sample cross-section. A total of ten sliced sections were investigated and the cross-sectional data of each tile was analysed using ImageJ [55–57]. The average measurement is then reported as the single number porosity of the coating. Further to optical microscopy, x-ray Diffractometry (XRD) was carried out to the investigate the phases present both on the powder and the coating. The XRD equipment of choice was the Regaku Ultima featuring a 3 kW x-ray generator at a 0.4 × 12 mm focus size.

SEM was carried out to study the materialography [58–60]of both the feedstock powder, coated sample, erodent and eroded surface. Lastly, the material composition of both the powder and the coated surface were investigated using the Energy Dispersive x-ray Spectroscopy (EDS). While there are numerous techniques [61–63] to prepare the sample for EDS, a mirror finish grade sequence mechanically polishing and hot resin mounting were the choice of procedure adopted in this study.

2.4. Hot air jet erosion

Hot air jet erosion was chosen to characterize the erosion performance of the coating to simulate an erosion environment close to that experienced by powder generation power plants or boiler flue tubes. According to a critical review of powerplant economizer tube failures carried out by Pal *et al* [64], a temperature of 417 °C is reported as the flue gas temperature. Consequently, hot air jet erosion of the NiCrSiB + 1.4 wt% nano-Al_2O_3 coated surface were carried out at a slightly higher temperature of 450 °C.

Alumina particles (50 μm avg.) featuring a flaky and angular morphology was the erodent of choice. The erosion tests were carried out at three impact angles between 30° and 90° at 30° intervals. The coated surface were exposed to the hot air jet for 10 min at an erodent feed rate and velocity of 5 g min^{-1} and 40 m s^{-1} respectively. The exit nozzle diameter was 1.5 mm placed at a distance of 10 mm (standoff) from the sample. The erosion rate (g/g) is evaluated as the ratio of erosion wear mass loss in grams to the mass of the erodent particle in grams. The tests were carried out following ASTMG76-18 [65, 66] using a Ducom air jet erosion tester.

3. Results and discussion

3.1. Analysis of the feedstock

From the scanning electron microscopy (SEM) data shown in figure 1., spheroidal particles can be observed for both of NiCrSiB (figure 1(a)) and nano-Al_2O_3 (figure 1(b)) which are critical for packing density. The bulk material density of the powders was 7715 kg m^{-3} for NiCrSiB and 3596 kg m^{-3} for nano-Al_2O_3.

When it comes to addition of nano particles, the maximum amount (wt%) of nano-Al_2O_3 powder that can be added NiCrSiB powder depends both on the particle diameter and the powder density. Consequently, this study adopts the nano (nm) to micron (μm) mass mixture ratio proposed by Wang *et al* [67] as shown in equation (1):

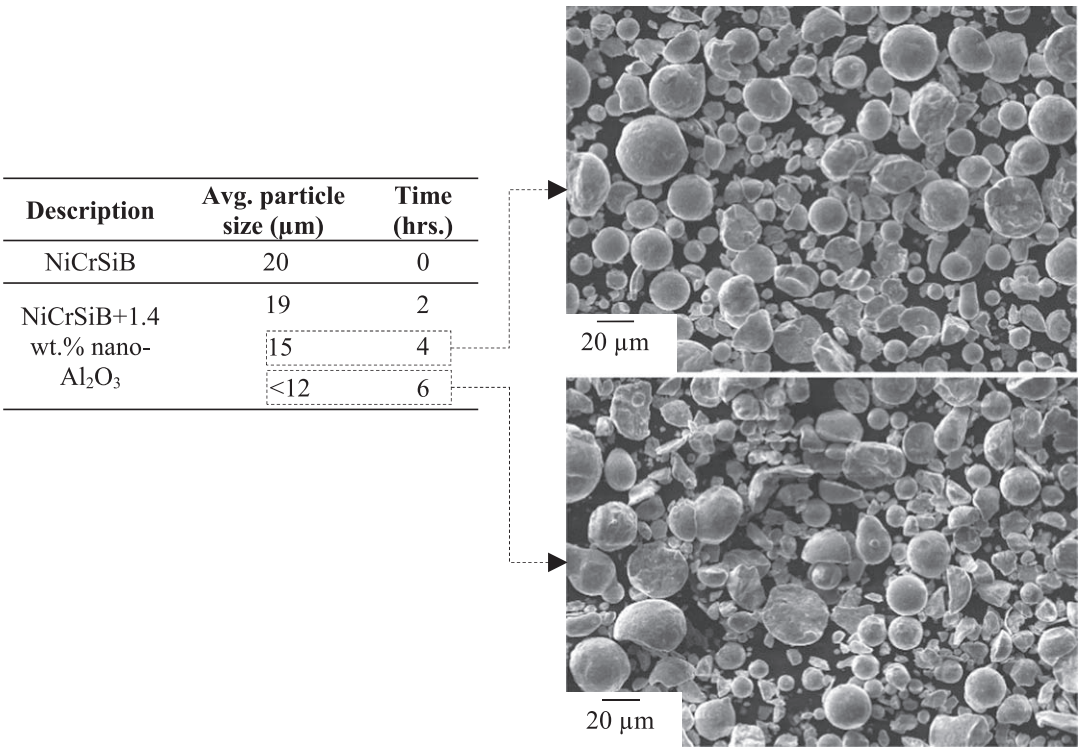

Figure 2. Influence of mechanical alloying milling time on the particle size of NiCrSiB + 1.4 wt% nano-Al_2O_3 powder.

$$\varepsilon_{wt} = \frac{d^3 g_n}{D^3 g_m}\left[\left(\frac{\pi}{\sqrt{3}}\right)\left(\frac{D}{d}+1\right)^2 + 0.026\left(\frac{D}{d}+2\right)^3\right] \quad (1)$$

where, ε_{wt} is the 'mixture mass ratio' of the respective micron and nano sizes feedstock powders. Accordingly, D is the average particle diameter of the micron powder and d is the diameter of the nano powder. Finally, the density of micron and nano powders are accounted as g_m (NiCrSiB) and g_n (nano-Al_2O_3) respectively.

Substituting the respective data to equation (1) reveleated that the maximum content (wt%) of nano-Al_2O_3 that can be added to micron-NiCrSiB is 1.4 wt%. Consequently, two proportion of mixing are considered in this study: the maximum limit and half, at of 1.4 wt% and 0.7 wt% of nano-Al_2O_3. The two cases (1.4 and 0.7) were considered in order to identify the influence of the nanoparticle quantity on the microstructure and surface properties of the resulting coating (micron-NiCrSiB + nano-Al_2O_3). The mechanical alloying of the feedstock powder mixture was carried out using a ball mill [68–70] featuring a planetary arrangement of 250 ml hardened steel vial and 10:1 powder to ball weight ratio at 250 rpm. In order to prevent excessive cold welding during the mechanical alloying process ethanol was used as the process control agent (PCA). Typically, ethanol is absorbed at the surfaces of the powdered particles and aids in reducing excessive cold welding between the powders along with the grinding medium and the milling container. This subsequently reduces agglomeration of particles which affects both flowability and the packing density. The mechanical alloying of all powder mixtures considered in this study were carried out in normal atmospheric conditions.

Figure 2 shows the influence of milling time on the particle size distribution (PSD) of the mechanically alloyed NiCrSiB + 1.4 wt% nano-Al_2O_3 powder. It can be seen that a 4-hrs. milling time yields a near normal PSD that is suitable for thermal spraying. Investigating the associated morphology through SEM shows that the particles are spherical and composed of a range of sizes which is beneficial both for powder flowability and splat density.

Excessive milling (6-hrs.) was found to causes fracturing of the Ni-based powder along with significant reduction in particle size (<12 μm). Further increments in grinding time will result in particle and grain sizes decreasing progressively with milling time, reaching nanometre levels. Consequently, mechanically alloyed powder post 4 h. were used as the feedstock for the HVOF process. Figure 3 shows the characteristics of the mechanically alloyed feedstock (NiCrSiB + 1.4 wt% nano-Al_2O_3). From the electron diffraction spectroscopy (EDS) analysis (figure 3), it was found that the mechanically alloyed composition is formed of nickel, aluminium, and chromium.

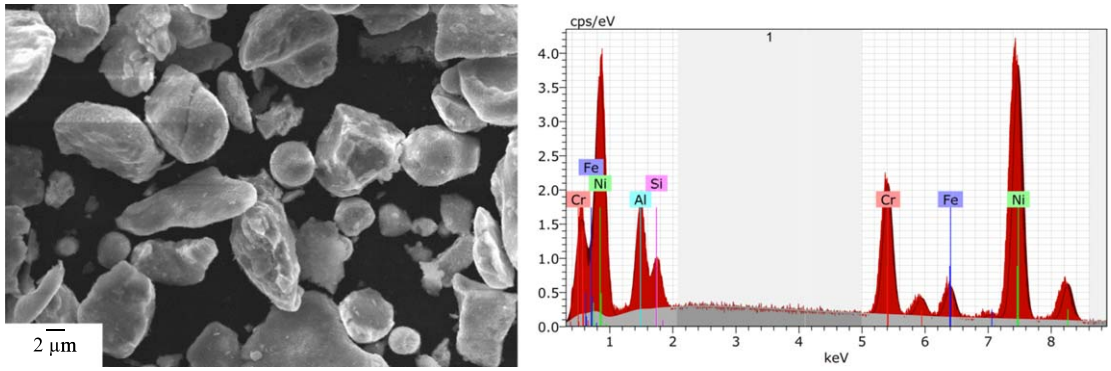

Figure 3. SEM and EDS of the mechanically alloyed NiCrSiB + 1.4 wt% nano-Al_2O_3 powder.

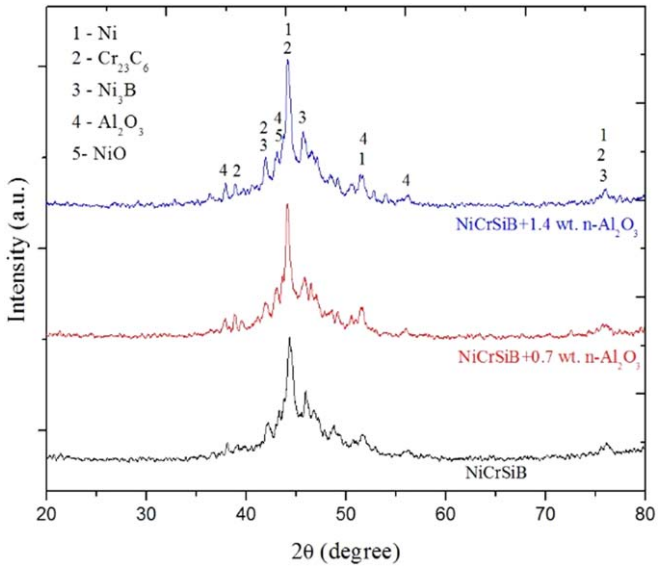

Figure 4. X-ray diffraction pattern of the NiCrSiB + 1.4 wt% nano-Al_2O_3 coating.

3.2. Characteristics of the 'NiCrSiB+nano-Al_2O_3' coating

XRD was conducted to assess the structure of NiCrSiB + 1.4 wt% nano-Al_2O_3 multilayer coating deposited on steel (AISI304) substrate (figure 4). The diffraction peaks were indexed by γ-Ni (JCPDS 04-0850) with traces of $Cr_{23}C_6$, Cr_7C_3, Ni_3B and Al_2O_3. However, the NiO component reveals that oxidation of the Ni particles has taken place as a result of the HVOF thermal spraying process. Furthermore, amorphisation can also be validated by the dimensional difference of the intensity peaks. The low intensity of Al_2O_3 peaks in the XRD pattern of NiCrSiB + 0.7 wt% nano-Al_2O_3, indicates either a low concentration of nanoparticles (that is below the XRD detection threshold) or that the nanoparticle have been fully melted as a result of the high-temperature facilitated by the HVOF flame decomposing to constituent elements.

To facilitate understanding of both the morphology and the composition of the coatings, the cross-sections were analysed and profiled using EDS. Three coating cases were considered as shown in figure 5, NiCrSiB, NiCrSiB + 0.7 wt% nano-Al_2O_3 and NiCrSiB + 1.4 wt% nano-Al_2O_3. The resulting elemental composition summarized in table 3. Figure 5(a) shows that the HVOF sprayed NiCrSiB coating is uniform and feature fewer number of pores. In the case of nano-Al_2O_3 added coatings (figures 5(b) and (c)), a lamellar structure of deformed dark Al_2O_3 reinforcing phase with grey Ni phase is formed.

The presence of pores and un-melted Al_2O_3 can be observed for both the cases (0.7 and 1.4 wt%) were nano-Al_2O_3 was added. The melting point of Al_2O_3 (2100 °C) is higher than that of Ni-base alloy (1040 °C–1200 °C), consequently, the Ni-base alloy powder and nano-Al_2O_3 particles can absorb sufficient heat for complete melting, extending and depositing to form a lamellar structure in the thermal spray process [32]. The number of lamellae was observed to be more in the 1.4 wt% nano-Al_2O_3 coating in comparison to the 0.7 wt%.

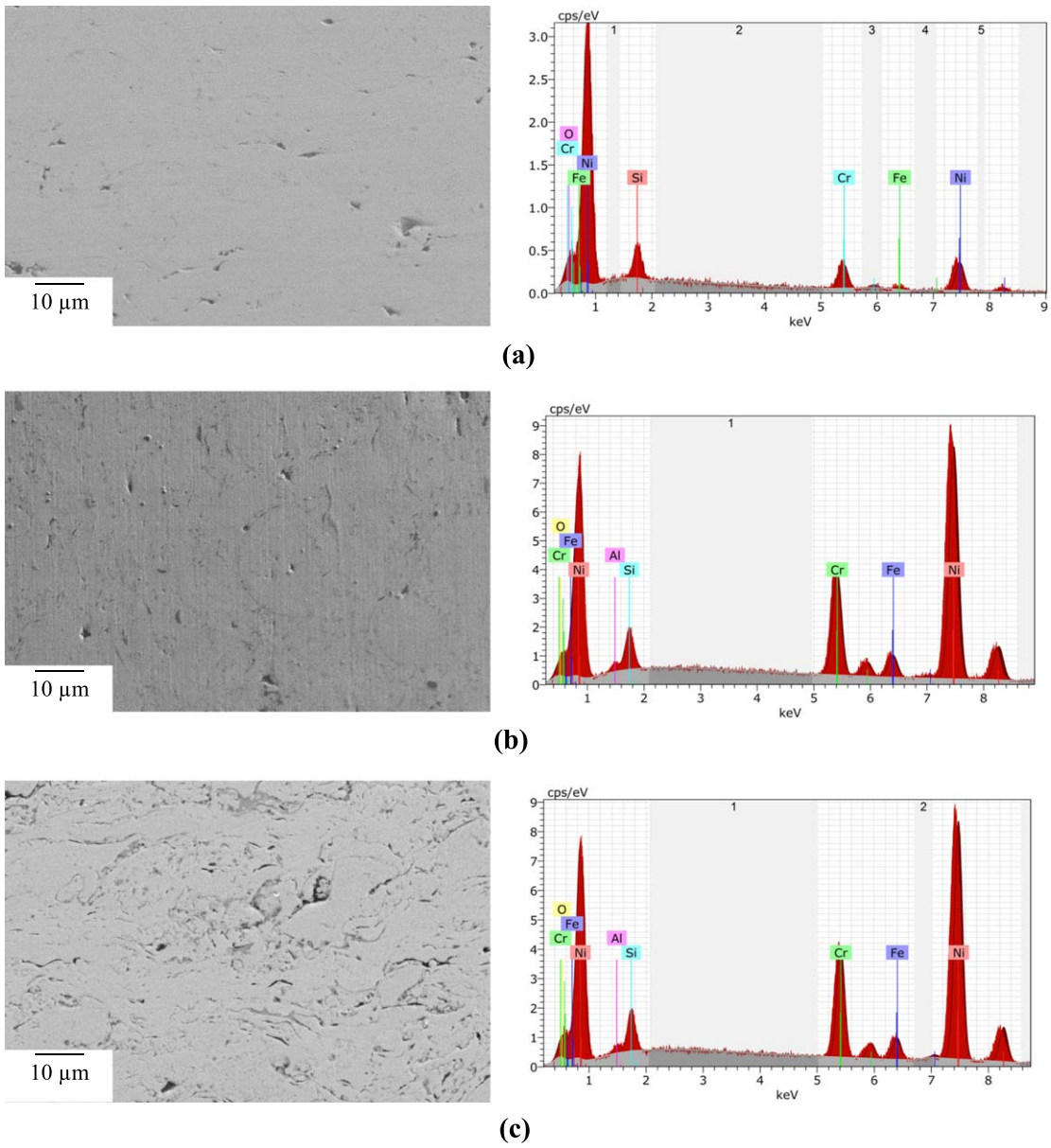

Figure 5. SEM informed cross-sectional morphology and the respective EDS spectrum of the coating showing (a) NiCrSiB, (b) NiCrSiB + 0.7 wt% nano-Al_2O_3 and (c) NiCrSiB + 1.4 wt% nano-Al_2O_3.

Table 3. Elemental composition deduced from EDS profiling of the respective coating cross-section.

Description	Si	Fe	Ni	Cr	O	Al	Total
NiCrSiB	7.99	2.99	43.47	16.25	29.31	—	100
NiCrSiB + 0.7 wt% nano-Al_2O_3	3.05	3.33	54.97	12.03	25.74	0.87	100
NiCrSiB + 1.4 wt% nano-Al_2O_3	3.69	3.95	49.35	15.20	26.75	1.06	100

Consequently, this effect can be attributed to the amount of nano-Al_2O_3 particle present in the feedstock mixture.

table 4 shows the results of porosity, surface roughness, microhardness, and adhesion strength. There is no significant variation observed in the porosity, surface roughness and adhesion strength with the addition of nano-Al_2O_3 particles. The adhesion strength from the stud pull off test was found to be in the range of 35–38 MPa for all the coating compositions tested. Investigating the macroscopic images of the failed samples as shown in figure 6, localised failing of the coating can be observed. Nevertheless, the major failure can be characterised as adhesion failure.

Table 4. Properties of the HVOF sprayed coatings.

Descriptions	NiCrSiB	NiCrSiB + 0.7 wt% nano-Al_2O_3	NiCrSiB + 1.4 wt% nano-Al_2O_3
Porosity (%)	1.5 ± 0.35	1.6 ± 0.4	1.8 ± 0.65
Surface roughness (μm)	6.2 ± 1.4	7.4 ± 1.2	8.5 ± 1.5
Microhardness ($HV_{0.3}$)	576 ± 40	620 ± 70	748 ± 80
Adhesion strength (MPa)	35 to 38		

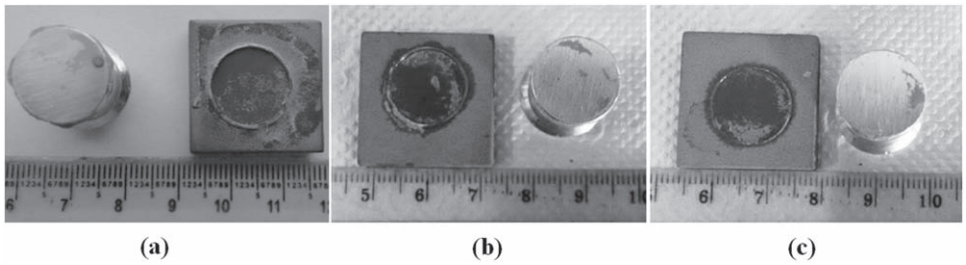

Figure 6. Failed samples post the adhesion strength test showing (a) NiCrSiB, (b) NiCrSiB + 0.7 wt% nano-Al_2O_3 and (c) NiCrSiB + 1.4 wt% nano-Al_2O_3.

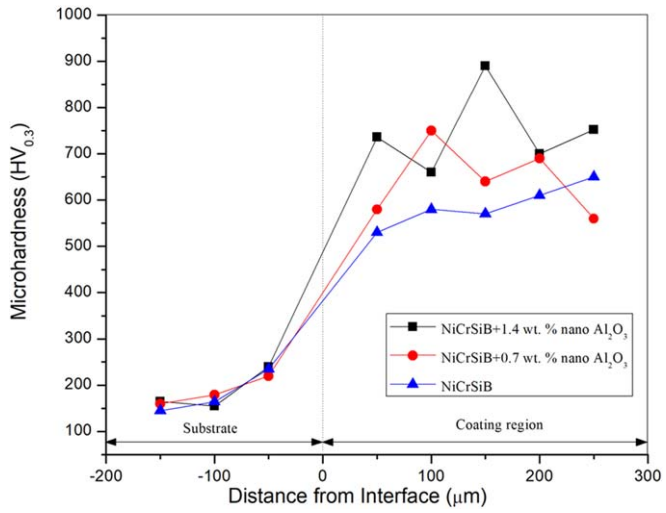

Figure 7. Microhardness performances of the coatings based on distance from the interface.

When Wang *et al* [71] and Yin *et al* [72] added Al_2O_3 to 75Ni and Al using HVOF and plasma spray respectively; an adhesion strength of 22.9 MPa and 28.8 MPa was observed. In comparison, it is clear that an improvement in adhesion strength (35–38 MPa) is obtained. The 20% improvement in adhesion strength can be attributed to increase in contact points facilitated by the well-flattened splats. This is a result of the high impact pressure of the melted/un-melted particles owing to the high impact velocity during HVOF spraying.

When it comes to the microhardness performance of the coating as shown in figure 7, the addition Al_2O_3 nanoparticles was found to have a significant effect (table 4). It was found that the microhardness of NiCrSiB coating increased with the addition of nano-Al_2O_3 as a result of the high hardness and compressive strength of the Al_2O_3 particles acting as a reinforcing phase. Furthermore, the Al_2O_3 addition also resulted in a good cohesive strength and lower porosity HVOF coating.

As listed in table 4, the highest microhardness (748 ± 80 $HV_{0.3}$) was observed for coating featuring the highest quantity of nano-Al_2O_3 (1.4 wt%), followed by 0.7% nano-Al_2O_3 (620 ± 70); a different of approximately 20%. Compared to the coating that featured NiCrSiB alone, this is an improvement of 30% at 1.4% addition of nano-Al_2O_3. Comparing the microhardness of the best performing coating (1.4 wt% nano-Al_2O_3) with that of literature as listed in table 5, an improvement in performance can be observed. It can be also seen that HVOF offers superior microhardness performance when adding Al_2O_3 in comparison to cold spray.

Table 5. Comparison of microhardness with relevant Al_2O_3 additions and NiCrSiB coatings found in literature.

References	Coating	Process	Microhardness
Grewal *et al* [28]	Ni + 40 wt% Al_2O_3	HVOF	714
Miguel *et al* [23]	NiCrSiB	Plasma sprayed	611
Wang *et al* [73]	NiAl + 40 wt% Al_2O_3	HVOF	411
Koivuluoto and Vuoristo [74]	NiCr + 50 wt% Al_2O_3	Cold spray	350
Hu *et al* [75]	Ni + 40 wt% Al_2O_3	Cold spray	225
Li *et al* [76]	Ni + Al_2O_3	Cold spray	173
This work	NiCrSiB + 1.4 wt% $_{nano\text{-}}Al_2O_3$	HVOF	748

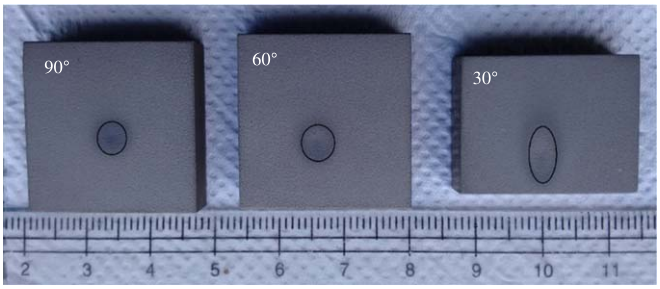

Figure 8. Samples post hot air jet erosion at 90°, 60°, and 30° impact angle.

3.3. Hot air jet erosion wear

Analysing the eroded sample post hot air jet erosion as shown in figure 8, a gradual reduction in wear scar can be observed as angle of impact increase. This shows that the mechanism of erosion is dependent on the process parameters involved. In the case of hot air jet erosion, it is primarily the impact angle when the erodent material is kept constant. This is because the impact angle can change the erosion behaviour of ductile and brittle materials [77]. Consequently, when the angle is lower, in this case 30°, the divergence of the alumina stream is higher, resulting in an elliptical shape as shown in figure 8; a case also reported by Laguna-Camacho *et al* [65]. This effect reduces as the erodent impact angle increases resulting in a comparatively smaller circular case at 90°. Nevertheless, in all the cases irrespective of the erodent angle, zonal erosion can be observed: these can be divided into areas of primary, secondary and tertiary erosion. The primary zone is where the erodent makes the first contact with the coating resulting in severe removal of the material, this was followed by an annular section where the erosion is medium followed by the and outside area where the erodent influence is minimum.

Classical analysis primarily refers to two classification of material removal from a coating under erosion ductile erosion and brittle erosion. However, according to Aquaro and Fontani [78], classification of ductile versus brittle erosion can be interchangeable based on the shift in peak erosion with respect to the impact angles and associated conditions. A 'ductile erosion' classification is appropriate when a higher wear rate occurs at low impact angles which then goes on to decrease as the impact angle increases. A brittle erosion on the contrary tend to peak at high angle of erodent impact subsequently being reduced as the impact angle decreases.

Comparing erosion performance of the coating as shown in figure 9, the erosion wear was found to be the highest at 30°, subsequently reaching the best performance at 90°. This clearly classifies that the erosion wear mechanism for all the coatings considered in this study are of a ductile nature. This also means that the shear strength of the coating is lower, and they have the capability to absorb a comparatively larger energy resulting from erodent at an impact angle of 90° as opposed to lower. The reason for this can be due to the presence of more Ni phase in the coatings. Overall, the results (figure 9) indicate that an addition of 1.4 wt% nano-Al_2O_3 improves the erosion resistance of NiCrSiB coatings up to 1.5 times at a 90° impact angle. Although a slight improvement in erosion resistance was observed at 0.7 wt% nano-Al_2O_3, the overall effect was found to be insignificant comparison to the performance of NiCrSiB alone.

3.4. Wear surface characterisation

The SEM worn surfaces of the coatings reveal the wear mechanism of NiCrSiB and NiCrSiB + 1.4 wt% nano-Al_2O_3 are shown in figures 10 and 11 respectively. Given that a sharp-edged and flaky alumina erodent is used, four major wear features can be observed: ploughing, microcutting, indentation and type I cutting. Comparatively, for the 1.4 wt% nano-Al_2O_3 addition, no long cracks could be observed, and the debris size is relatively small with significant fracturing of silica. This reflects the good adhesion between nanoparticles and

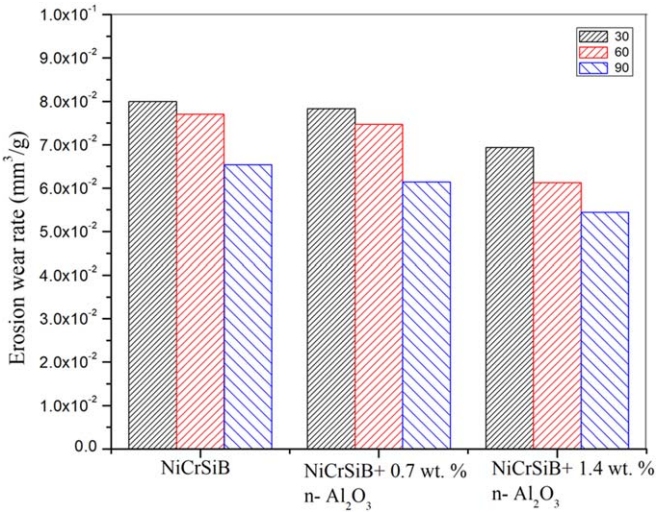

Figure 9. Rate of erosion wear observed for respective coatings at 90°, 60°, and 30° impact angles.

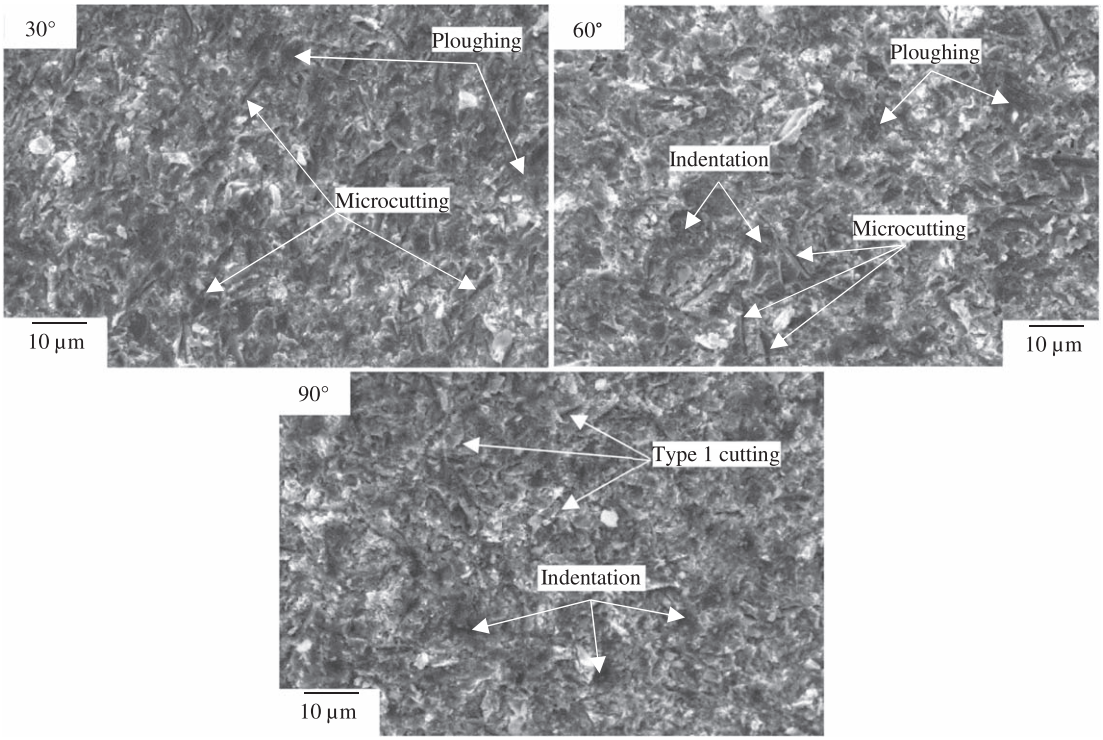

Figure 10. Wear characteristics observed at the surface of the HVOF sprayed NiCrSiB coating post hot air jet erosion at the respective angle of impact.

the NiCrSiB. There are numerous thoughts reported on the mechanism of erosion wear in coatings [79]. It is generally considered that at oblique erodent impact, wear happens primarily as a result of cutting action of the particle irrespective of its shape and size. Consequently, material removal by oblique cutting action can be observed primarily at 30° and 60° impact angles. The material is removed by a ploughing action, displacing materials to the front and side of the particle. Further impacts on the neighbouring site cause removal of highly strained materials from the rim or terminal lip of the crater.

When the alumina particle rolls forwards post-contact with the surface, material is removed by repeated impacts on a prominent lip formed by the indenting angular particle and this is termed type I cutting which can be observed at higher angles. Material removal 90° shows indentions and craters which is a result of localised strain. The extruded rim of material that an bee seen around the craters further validates that a ductile wear is taking place.

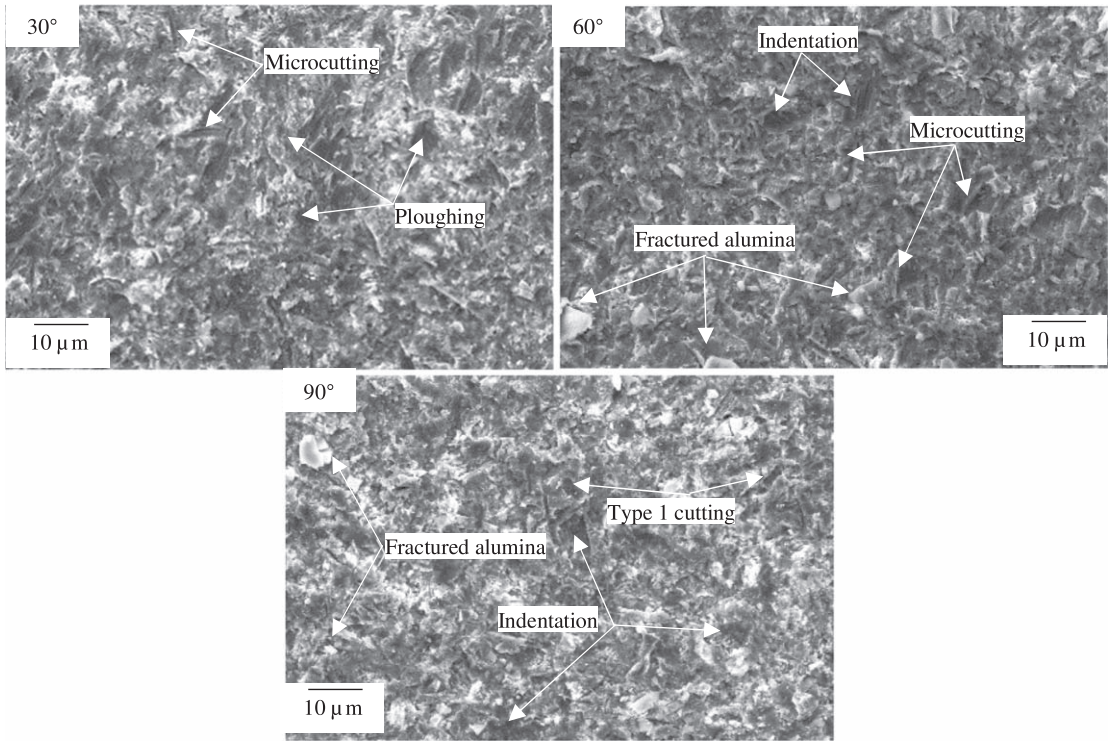

Figure 11. Wear characteristics observed at the surface of the HVOF sprayed of NiCrSiB + 1.4 wt% nano-Al_2O_3 coating post hot air jet erosion at the respective angle of impact.

In addition to the microcutting and ploughing, the material loss in NiCrSiB + 1.4 wt% nano-Al_2O_3 was due to the fracturing and pull of the Al_2O_3 splat. At 90° impact angle, the impact energy reaches a maximum and causes extensive indentation deformation accompanied with the formation of dislocations. The accumulation of dislocations due to the further impact of the erodent particle, accelerates the Al_2O_3 splat pull out at the weak bonding boundaries. The fracturing of the Al_2O_3 splat was attributed to the intersection of lateral cracks formed due to the indentation of irregularly shaped alumina erodent particles on the brittle Al_2O_3 splat on the coating. Consequently, the addition of 1.4 wt% nano-Al_2O_3 to NiCrSiB (figure 10) show better erosion resistance as compared to NiCrSiB coating (figure 11), primarily attributable to the 'pinning effect' of the hard Al_2O_3 particles with higher hardness in the coating in spite of fracturing and pull off of the Al_2O_3 splat. The large concentration of the fractured alumina observed in figure 11 also shows the improved hardness of the surface.

In summary, the erosion of NiCrSiB coating post hot air jet alumina erodent involves wear by cutting mechanism observed in ductile mode of erosion mechanism (ploughing, microcutting, indentation, type 1). For the case of NiCrSiB + 1.4 wt% nano-Al_2O_3 coating, the fracturing and pull out of the alumina splat observed shows that, even though a ductile mechanism dominates the wear mechanism partial brittle modes are also prevalent. Nevertheless, the best performance for all coatings were observed at perfectly axial impact of erodent (90°) in comparison to oblique angles (30° and 60°) primarily due to the high volumes of Ni-metallic phase.

4. Conclusions

The study demonstrates the development of NiCrSiB/nano-Al_2O_3 HVOF coating deposited on a steel (AISI304) substrate. In addition to characterising the erosion wear mechanism, the influence of nano-Al_2O_3 on the microstructure and surface properties are presented. A 4 h. mechanically alloying was found to be most suitable to obtain a near normal particle size distribution (PSD) when incorporate 1.4 wt% nano-Al_2O_3 with NiCrSiB for HVOF thermal spraying. The resulting microstructure of the coating consists primarily of Ni, $Cr_{23}C_6$, and Cr_5B_3 phases with minor phases of alumina and NiO. Overall, no significant variation in porosity, surface roughness and adhesion strength of NiCrSiB coatings was observed as a result of adding either 0.7 or 1.4 wt% nano-Al_2O_3. However, the microhardness of the NiCrSiB coating increased significantly from 576 $HV_{0.3}$ to 748 $HV_{0.3}$ when 1.4 wt% addition of nano-Al_2O_3 to the NiCrSiB feedstock. Furthermore, the erosions resistance of NiCrSiB coating improved up to 1.5 times at 90° erodent impact as a result of 1.4 wt% addition of nano-Al_2O_3. Even though, the ductile mechanism (ploughing, microcutting, indentation, type-I cutting) was the most prevalent

erosion mechanism, the addition of nano-Al_2O_3 was found to show certain brittle characteristics such as mild cracking and pull out of the alumina hard phase.

ORCID iDs

Ayyappan Susila Praveen https://orcid.org/0000-0001-5877-3805
Arun Arjunan https://orcid.org/0000-0001-5493-0957

References

[1] Li X, Ding H, Huang Z, Fang M, Liu B, Liu Y, Wu X and Chen S 2014 Solid particle erosion-wear behavior of SiC-Si3N4 composite ceramic at elevated temperature *Ceram. Int.* **40** 16201–7
[2] Cai F, Huang X and Yang Q 2015 Mechanical properties, sliding wear and solid particle erosion behaviors of plasma enhanced magnetron sputtering CrSiCN coating systems *Wear* **324–325** 27–35
[3] Swain B, Patnaik A, Bhuyan S K, Barik K N, Sethi S K, Samal S, Mishra S C and Behera A 2018 Solid particle erosion wear on plasma sprayed mild steel and copper surface *Mater. Today Proc.* 3 **5** pp 20403–12 Elsevier Ltd
[4] Sundararajan G and Roy M 1997 Solid particle erosion behaviour of metallic materials at room and elevated temperatures *Tribol. Int.* **30** 339–59
[5] Sidhu T S, Malik a, Prakash S and Agrawal R D 2007 Oxidation and hot corrosion resistance of HVOF WC-NiCrFeSiB coating on Ni- and Fe-based superalloys at 800 °C *J. Therm. Spray Technol.* **16** 844–9
[6] Martinella R 1990 Solid particle erosion in electric power plants *Vib. Wear High Speed Rotating Mach.* (Netherlands: Springer) pp 339–83
[7] Basu P, Kefa C and Jestin L 2000 *Erosion Prevention in Boilers* (*Boilers and Burners* Mechanical Engineering Series) (New York: Springer) 426–56
[8] Hidalgo V H, Varela J B, Menéndez A C and Martínez S P 2001 High temperature erosion wear of flame and plasma-sprayed nickel-chromium coatings under simulated coal-fired boiler atmospheres *Wear* **247** 214–22
[9] Ramesh M R, Prakash S, Nath S K, Sapra P K and Venkataraman B 2010 Solid particle erosion of HVOF sprayed WC-Co/NiCrFeSiB coatings *Wear* **269** 197–205
[10] Springthorpe M, Hasan S and Arjunan A 2017 The role of coatings on corrosion resistance of aerospace aluminum alloys *Adv. Mater. Process. Technol. (AMPT) (11th to 14th December 2017) (Chennai, India, AMPT, Chennai*
[11] Sahu S P, Satapathy A, Patnaik A, Sreekumar K P and Ananthapadmanabhan P V 2010 Development, characterization and erosion wear response of plasma sprayed fly ash-aluminum coatings *Mater. Des.* **31** 1165–73
[12] Vicenzi J, Villanova D L, Lima M D, Takimi A S, Marques C M and Bergmann C P 2006 HVOF-coatings against high temperature erosion (~300 °C) by coal fly ash in thermoelectric power plant *Mater. Des.* **27** 236–42
[13] Wang B Q 1995 Erosion-corrosion of coatings by biomass-fired boiler fly ash *Wear* **188** 40–8
[14] Rao B G, Mukherjee D and Reddy B M 2017 Novel approaches for preparation of nanoparticles *Nanostructures Nov. Ther. Synth. Charact. Appl* (Amsterdam: Elsevier Inc) pp 1–36
[15] Henao J, Poblano-Salas C, Monsalve M, Corona-Castuera J and Barceinas-Sanchez O 2019 Bio-active glass coatings manufactured by thermal spray: a status report *J. Mater. Res. Technol.* **8** 4965–84
[16] Ghadami F and Aghdam A S R 2019 Improvement of high velocity oxy-fuel spray coatings by thermal post-treatments: a critical review *Thin Solid Films* **678** 42-52
[17] Pawlowski L 2008 *The Science and Engineering of Thermal Spray Coatings* (The Atrium, Southern Gate, Chichester, West Sussex PO19 8SQ, England: Wiley)
[18] Fauchais P L, Heberlein J V R and Boulos M I 2014 *Thermal Spray Fundamentals* (New York: Springer Science + Business Media) Springer Science+Business Media (https://doi.org/10.1007/978-0-387-68991-3)
[19] Maranho O, Rodrigues D, Boccalini M and Sinatora A 2008 Influence of parameters of the HVOF thermal spray process on the properties of multicomponent white cast iron coatings *Surf. Coatings Technol.* **202** 3494–500
[20] Mohammadi M, Javadpour S, Jahromi S A J, Shirvani K and Kobayashi A 2012 Characterization and hot corrosion performance of LVPS and HVOF-CoNiCrAlYSi coatings *Vacuum* **86** 1458–64
[21] Praveen A S and Arjunan A 2019 Parametric optimisation of high-velocity oxy-fuel nickel-chromium-silicon-boron and aluminium-oxide coating to improve erosion wear resistance *Mater. Res. Express* **6** 096560
[22] Saaedi J, Coyle T W, Arabi H, Mirdamadi S and Mostaghimi J 2010 Effects of HVOF process parameters on the properties of Ni-Cr coatings *J. Therm. Spray Technol.* **19** 521–30
[23] Miguel J M, Guilemany J M and Vizcaino S 2003 Tribological study of NiCrBSi coating obtained by different processes *Tribol. Int.* **36** 181–7
[24] Serres N, Hlawka F, Costil S, Langlade C, Machi F and Cornet A 2009 Dry coatings and ecodesign: I. environmental performances and chemical properties *Surf. Coatings Technol.* **204** 187–96
[25] Kawahara Y 2007 Application of high temperature corrosion-resistant materials and coatings under severe corrosive environment in waste-to-energy boilers *J. Therm. Spray Technol.* **16** 202–13
[26] Simunovic K, Saric T and Simunovic G 2014 Different approaches to the investigation and testing of the ni-based self-fluxing alloy coatings—a review. Part 1: general facts, wear and corrosion investigations *Tribol. Trans.* **57** 955–79
[27] Tobar M J, Álvarez C, Amado J M, Rodríguez G and Yáñez A 2006 *Morphology and Characterization of Laser Clad Composite NiCrBSi—WC Coatings on Stainless Steel* **200** 6313–7
[28] Grewal H S, Singh H and Agrawal A 2013 Microstructural and mechanical characterization of thermal sprayed nickel-alumina composite coatings *Surf. Coatings Technol.* **216** 78–92
[29] Harsha S, Dwivedi D K and Agarwal A 2008 Influence of CrC addition in Ni-Cr-Si-B flame sprayed coatings on microstructure, microhardness and wear behaviour *Int. J. Adv. Manuf. Technol.* **38** 93–101
[30] Cai B, Tan Y F, He L, Tan H and Gao L 2013 Tribological properties of TiC particles reinforced Ni-based alloy composite coatings *Trans. Nonferrous Met. Soc. China (English Ed.* **23** 1681–8

[31] Määttä A, Kanerva U and Vuoristo P 2011 Structure and tribological characteristics of HVOF coatings sprayed from powder blends of Cr 3C 2-25NiCr and NiCrBSi alloy *J. Therm. Spray Technol.* **20** 366–71

[32] He L, Tan Y, Wang X, Xu T and Hong X 2014 Microstructure and wear properties of Al_2O_3-CeO_2/Ni-base alloy composite coatings on aluminum alloys by plasma spray *Appl. Surf. Sci.* **314** 760–7

[33] Liu F, Fang M, Huang Z, Liu Y and Huang S 2012 Preparation and mechanical properties of NiCr—Al_2O_3—ZrO_2(8Y) ceramic composites *Mater. Sci. Eng.* A **554** 1–5

[34] Fernandes F, Ramalho A, Loureiro A, Guilemany J M, Torrell M and Cavaleiro A 2013 Influence of nanostructured ZrO_2 additions on the wear resistance of Ni-based alloy coatings deposited by APS process *Wear* **303** 591–601

[35] Hou Q Y, Huang Z and Wang J T 2011 Influence of nano-Al_2O_3 particles on the microstructure and wear resistance of the nickel-based alloy coating deposited by plasma transferred arc overlay welding *Surf. Coatings Technol.* **205** 2806–12

[36] Xu J, Tao J and Jiang S 2008 Microstructure and properties of nano-Al_2O_3 particle reinforced Ni–Cr–Mo–Cu composite alloying layer *Mater. Chem. Phys.* **112** 966–72

[37] Wang H Y, Zuo D W, Di Wang M, Sun G F, Miao H and Sun Y L 2011 High temperature frictional wear behaviors of nano-particle reinforced NiCoCrAlY cladded coatings *Trans. Nonferrous Met. Soc. China (English Ed.* **21** 1322–8

[38] Zhang S, Li M, Yoon J H, Cho T Y, Lee C G and He Y 2008 The comparative study on microstructure and properties of nano-CeO_2 and Sm_2O_3 particulate reinforced nickel-based composites by laser deposition *Appl. Surf. Sci.* **254** 7446–52

[39] Liu L and Xu J 2011 A study of the erosion-corrosion behavior of nano-Cr_2O_3 particles reinforced Ni-based composite alloying layer in aqueous slurry environment *Vacuum* **85** 687–700

[40] Wang H Y, Zuo D W, Sun Y L, Xu F and Zhang D 2009 Microstructure of nanometer Al_2O_3 dispersion strengthened Ni-based high-temperature protective coatings by laser cladding *Trans. Nonferrous Met. Soc. China (English Ed.* **19** 586–91

[41] Liu S L, Zheng X P and Geng G Q 2010 Influence of nano-WC-12Co powder addition in WC-10Co-4Cr AC-HVAF sprayed coatings on wear and erosion behaviour *Wear* **269** 362–7

[42] Uusitalo M A, Vouristo P M J and Mäntylä T A 2003 High temperature corrosion of coatings and boiler steels in oxidizing chlorine-containing atmosphere *Mater. Sci. Eng.* A **346** 168–77

[43] Kumar S, Kumar M and Handa A 2018 Combating hot corrosion of boiler tubes—a study *Eng. Fail. Anal.* **94** 379–95

[44] Sen D, Chavan N M, Rao D S and Sundararajan G 2010 Influence of grit blasting on the roughness and the bond strength of detonation sprayed coating *J. Therm. Spray Technol.* **19** 805–15

[45] Wang Y Y, Li C J and Ohmori A 2005 Influence of substrate roughness on the bonding mechanisms of high velocity oxy-fuel sprayed coatings *Thin Solid Films* **485** 141–7

[46] ASTM C1070, ASTM C1070 - 01(2014) 2014 Standard Test Method for Determining Particle Size Distribution of Alumina or Quartz by Laser Light Scatteringhttps://astm.org/Standards/C1070.htm(accessed November 23, 2019)

[47] Dolatabadi A, Pershin V and Mostaghimi J 2005 New attachment for controlling gas flow in the HVOF process *J. Therm. Spray Technol.* **14** 91–9

[48] Liu M, Yu Z, Zhang Y, Wu H, Liao H and Deng S 2019 Prediction and analysis of high velocity oxy fuel (HVOF) sprayed coating using artificial neural network *Surf. Coatings Technol.* **378** 124988

[49] Vicenzi J, Marques C M and Bergmann C P 2008 Hot and cold erosive wear of thermal sprayed NiCr-based coatings: influence of porosity and oxidation *Surf. Coatings Technol.* **202** 3688–97

[50] Poirier D, Legoux J G and Lima R S 2012 Engineering HVOF-sprayed Cr_3C_2-NiCr coatings: the effect of particle morphology and spraying parameters on the microstructure, properties and high temperature wear performance *Proc. Int. Therm. Spray Conf.* (ASM Int.) pp 22–7

[51] Matikainen V, Bolelli G, Koivuluoto H, Honkanen M, Vippola M, Lusvarghi L and Vuoristo P 2017 A study of Cr_3C_2-based HVOF- and HVAF-sprayed coatings: microstructure and carbide retention *J. Therm. Spray Technol.* **26** 1239–56

[52] Kang A S, Grewal J S and Cheema G S 2017 Effect of thermal spray coatings on wear behavior of high tensile steel applicable for tiller blades *5th International Conference of Materials Processing and Characterization (ICMPC 2016)* 4 (*Materials Today Proceedings* 2) (Amsterdam: Elsevier Ltd) pp 95–103

[53] Vashishtha N, Khatirkar R K and Sapate S G 2017 Tribological behaviour of HVOF sprayed WC-12Co, WC-10Co-4Cr and Cr_3C_2−25NiCr coatings *Tribol. Int.* **105** 55–68

[54] Elmoursi A. a. and Patel N 2004 Adhesion measurement procedures for kinetic and thermal spray coatings using a stud-pull tester *J. Adhes. Sci. Technol.* **18** 597–606

[55] Arjunan A 2019 Acoustic absorption of passive destructive interference cavities *Mater. Today Commun.* **19** 68–75

[56] Arjunan A, Wang C J, Yahiaoui K, Mynors D J, Morgan T, Nguyen V B and English M 2014 Sound frequency dependent mesh modelling to simulate the acoustic insulation of stud based double-leaf walls *Proc. ISMA 2014 - Int. Conf. Noise Vib. Eng. USD 2014 - Int. Conf. Uncertain. Struct. Dyn.*

[57] Arjunan A 2019 Targeted sound attenuation capacity of 3D printed noise cancelling waveguides *Appl. Acoust.* **151** 30–44

[58] Bari K and Arjunan A 2019 Extra low interstitial titanium based fully porous morphological bone scaffolds manufactured using selective laser melting *J. Mech. Behav. Biomed. Mater.* **95** 1–12

[59] Vance A, Bari K and Arjunan A 2019 Investigation of Ti64 sheathed cellular anatomical structure as a tibia implant *Biomed. Phys. Eng. Express* **5** 035008

[60] Vance A, Bari K and Arjunan A 2018 Compressive performance of an arbitrary stiffness matched anatomical Ti64 implant manufactured using direct metal laser sintering *Mater. Des.* **160** 1281–94

[61] Walck S 2013 Sample preparation considerations for x-ray EDS analysis in the physical sciences *Microsc. Microanal.* **19** 2012–3

[62] Arjunan A, Demetriou M, Baroutaji A and Wang C 2020 Mechanical performance of highly permeable laser melted Ti6Al4V bone scaffolds *J. Mech. Behav. Biomed. Mater.* **102** 103517

[63] Arjunan A, Baroutaji A, Praveen A S, Olabi A G and Wang C J 2019 Acoustic performance of metallic foams *Ref. Modul. Mater. Sci. Mater. Eng.* (Amsterdam: Elsevier) (https://doi.org/10.1016/B978-0-12-803581-8.11561-9)

[64] Pal U, Kishore K, Mukhopadhyay S, Mukhopadhyay G and Bhattacharya S 2019 Failure analysis of boiler economizer tubes at power house *Eng. Fail. Anal.* **104** 1203–10

[65] Laguna-Camacho J R, Marquina-Chávez a, Méndez-Méndez J V, Vite-Torres M and Gallardo-Hernández E. a. 2013 Solid particle erosion of AISI 304, 316 and 420 stainless steels *Wear* **301** 398–405

[66] ASTM G76-18 2018 Standard Test Method for Conducting Erosion Tests by Solid Particle Impingement Using Gas Jets, ASTM International, West Conshohocken, PA, 2018. DOI: 10.1520/G0076-18

[67] Wang H Y, Zuo D W, Yu S X and Zhang D 2009 Preparation process of metal matrix micro/nano-powders reinforced by nanometer particles *Adv. Mater. Res.* **60–6 1** 155–9

[68] Prasad C D, Joladarashi S, Ramesh M R, Srinath M S and Channabasappa B H 2018 Influence of microwave hybrid heating on the sliding wear behaviour of HVOF sprayed CoMoCrSi coating *Mater. Res. Express* **5** 086519
[69] Prasad C D, Joladarashi S, Ramesh M R, Srinath M S and Channabasappa B H 2019 Microstructure and tribological behavior of flame sprayed and microwave fused CoMoCrSi/CoMoCrSi-Cr_3C_2 coatings *Mater. Res. Express* **6** 026512
[70] Prasad C D, Joladarashi S, Ramesh M R, Srinath M S and Channabasappa B H 2019 Effect of microwave heating on microstructure and elevated temperature adhesive wear behavior of HVOF deposited CoMoCrSi-Cr_3C_2 coating *Surf. Coatings Technol.* **374** 291–304
[71] Wang Y-Y, Li C-J and Ohmori A 2006 Examination of factors influencing the bond strength of high velocity oxy-fuel sprayed coatings *Surf. Coatings Technol.* **200** 2923–8
[72] Yin Z, Tao S, Zhou X and Ding C 2008 Microstructure and mechanical properties of Al_2O_3-Al composite coatings deposited by plasma spraying *Appl. Surf. Sci.* **254** 1636–43
[73] Wang B and Lee S W 2000 Erosion-corrosion behaviour of HVOF NiAl-Al_2O_3 intermetallic-ceramic coating *Wear* **239** 83–90
[74] Koivuluoto H and Vuoristo P 2009 Effect of ceramic particles on properties of cold-sprayed ni-20cr+al 2o 3 coatings *J. Therm. Spray Technol.* **18** 555–62
[75] Hu H X, Jiang S L, Tao Y S, Xiong T Y and Zheng Y G 2011 Cavitation erosion and jet impingement erosion mechanism of cold sprayed Ni-Al_2O_3 coating *Nucl. Eng. Des.* **241** 4929–37
[76] Li W Y, Zhang C, Liao H, Li J and Coddet C 2008 Characterizations of cold-sprayed Nickel-Alumina composite coating with relatively large Nickel-coated Alumina powder *Surf. Coatings Technol.* **202** 4855–60
[77] Landolt D and Mischler S 2011 *Tribocorrosion of Passive Metals and Coatings* (Cambridge: Woodhead Publishing) 978-1-84569-966-6
[78] Aquaro D and Fontani E 2001 Erosion of ductile and brittle materials *Meccanica* **36** 651–61
[79] Hutchings I and Shipway P 2017 Wear by hard particles *Tribology* (Amsterdam: Elsevier) pp 165–236